JOURNAL OF SYNCHROTRON RADIATION
ISSN 1600-5775

Structural investigation of m*M* Ni(II) complex isomers using transmission XAFS: the significance of model development

M. Tauhidul Islam,[a,b] Christopher T. Chantler,[a]* Mun Hon Cheah,[c] Lachlan J. Tantau,[a] Chanh Q. Tran[d] and Stephen P. Best[b]

[a]School of Physics, University of Melbourne, Australia, [b]School of Chemistry, University of Melbourne, Australia, [c]ANU College of Medicine, Biology and Environment, Australian National University, Australia, and [d]School of Physics, La Trobe University, Australia. *Correspondence e-mail: chantler@unimelb.edu.au

Received 7 July 2015
Accepted 10 August 2015

Keywords: XAFS with uncertainty; hybrid technique; transmission XAFS; nickel(II) complexes.

High-accuracy transmission XAFS determined using the hybrid technique has been used to refine the geometries of bis(*N*-n-propyl-salicylaldiminato) nickel(II) (n-pr Ni) and bis(*N*-i-propyl-salicylaldiminato) nickel(II) (i-pr Ni) complexes which have approximately square planar and tetrahedral metal coordination. Multiple-scattering formalisms embedded in *FEFF* were used for XAFS modelling of the complexes. Here it is shown that an *IFEFFIT*-like package using weighting from experimental uncertainty converges to a well defined XAFS model. Structural refinement of (i-pr Ni) was found to yield a distorted tetrahedral geometry providing an excellent fit, $\chi_r^2 = 2.94$. The structure of (n-pr Ni) is best modelled with a distorted square planar geometry, $\chi_r^2 = 3.27$. This study demonstrates the insight that can be obtained from the propagation of uncertainty in XAFS analysis and the consequent confidence which can be obtained in hypothesis testing and in analysis of alternate structures *ab initio*. It also demonstrates the limitations of this (or any other) data set by defining the point at which signal becomes embedded in noise or amplified uncertainty, and hence can justify the use of a particular *k*-range for one data set or a different range for another. It is demonstrated that, with careful attention to data collection, including the correction of systematic errors with statistical analysis of uncertainty (the hybrid method), it is possible to obtain reliable structural information from dilute solutions using transmission XAFS data.

1. Introduction

The facile change in coordination number and geometry and their inter-related redox behaviour contribute to the function of transition metals as the catalyst of choice in most biological and abiological systems. The characterization of transition metal complexes in contexts relevant to those of the operating catalyst is as technically demanding as it is important. In cases where the complex is able to be isolated in crystalline form, X-ray crystallography, electron diffraction or neutron diffraction can be applied to reveal the structure with often exquisite accuracy and precision (Takayanagi *et al.*, 1985; Harper *et al.*, 2006; Steiner & Saenger, 1992; Langford & Louër, 1996). However, two limitations of the approach remain: the first centres on cases where the complex is not able to be isolated in crystalline form (Anderson, 1975; Bart, 1986); the second is concerned with the validity of the X-ray structure to contexts relevant to the catalytic system. In this latter context, X-ray absorption fine structure (XAFS) (Eisenberger & Kincaid, 1978) can be advantageous and ideally suited. Extended X-ray absorption fine structure (EXAFS), the

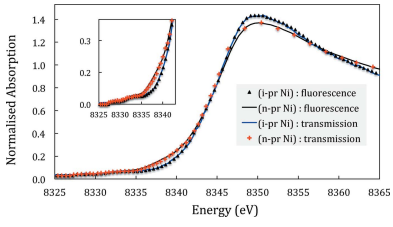

oscillatory part in the X-ray absorption spectra (XAS) above an X-ray absorption edge (Lytle *et al.*, 1975), can provide information in the vicinity of atoms in a wide variety of gaseous, solid and liquid systems. In addition, the sensitivity of XAFS to the local environment allows for subtle stereochemical analyses of chemically important compounds or complexes (Chantler *et al.*, 2012; Mazzara *et al.*, 2000; Perutz *et al.*, 1982; Yamaguchi *et al.*, 1982).

Unlike X-ray crystallography, where there is a robust and widely accepted statistical basis for the evaluation of derived structures, error analysis of EXAFS data is in most cases limited to a simple assessment based on the variance of repeated measurements, assignment of errors based on the k value of the data or, worse, set to a constant value (that is, ignored). Consequently, the normal statistical measures of the reliability of a derived result are of limited or no use. We have shown that, if accuracy (or even precision) is determined experimentally, additional structural insight associated with XAFS refinement statistics can be obtained (Chantler *et al.*, 2012), leading to the determination of structural geometry with quantified certainty.

There are now well established protocols for the determination of EXAFS data with well defined accuracy and precision for transmittance measurements from concentrated (ideal) solids (Chantler, 2009). Our research program sets out to extend the application of those approaches to the study of dilute samples with the absorber in an aperiodic environment. In this contribution we examine the EXAFS of dilute solutions of isomeric nickel(II) complexes with salicylaldiminato ligands which differ in terms of the stereochemistry of the complex. The aims of the work are: (i) to extract EXAFS with defined accuracy and to apply these data to a statistically robust analysis; (ii) to evaluate the robustness of statistical measures of the quality of fit when evaluating the models used to describe the EXAFS; (iii) to establish whether transmission measurements from dilute samples can be used to determine the stereochemistry of metal complexes with good statistical reliability; and (iv) to establish whether there are statistically significant differences between X-ray crystalline and solution structures of the square planar and tetrahedral nickel(II) complexes.

1.1. Overview

The complexes bis(*N*-i-propyl-salicyldiminato) nickel(II), (i-pr Ni), and bis(*N*-n-propyl-salicylaldiminato) nickel (II), (n-pr Ni), are well known to give local metal environments having approximate tetrahedral (Fox *et al.*, 1963, 1964) and square planar coordination (Britton & Pignolet, 1989) geometries. The solid state structures have been studied by X-ray crystallography and the differing magnetic properties of d^8 square planar and tetrahedral complexes can be used to confirm that the solid-state structures are in general terms retained in solution.

Consequently, the pair of nickel complexes provide an excellent vehicle to examine the limits of X-ray spectroscopy and EXAFS analysis for the resolution of structural questions. The underlying question explored in this contribution is whether statistically meaningful structural information can be obtained from transmission EXAFS measurements from absorbers in dilute concentration in an aperiodic environment. First we address the question whether the X-ray derived structures provide a sufficient or satisfactory description of the complexes in (frozen) solution. We then build structural models from knowledge of the ligand to examine whether the statistical measures of the agreement between the calculated and observed EXAFS are sufficient to prove the stereochemistry of the salicyldiminato ligands bound to the nickel.

2. Data for this analysis

X-ray absorption spectra of (i-pr Ni) and (n-pr Ni) complexes, and their corresponding metallic Ni element, were determined with defined accuracy from the measured intensities using multiple solutions for each of the complexes. For each isomer, spectra were obtained in step-scan mode where three sample positions (comprising blank, 1.5 and 15 m*M* solutions of the complex) were measured at each energy (Chantler *et al.*, 2015).

Data on key experimental systematics including energy calibration, dark current, harmonic contamination and scattering were measured and the spectra corrected using published procedures (Islam *et al.*, 2014; Glover & Chantler, 2009; Tantau *et al.*, 2015; Tran *et al.*, 2004; Barnea *et al.*, 2011). Detailed analytical methodologies are addressed by Chantler *et al.* (2015). Corrected X-ray absorption spectra of the two complexes from 15 m*M* solution, and of the corresponding element, *i.e.* Ni, shown in Fig. 1, were converted into χ *versus* k spectra with the propagation of experimental uncertainty using the methods outlined in the following sections.

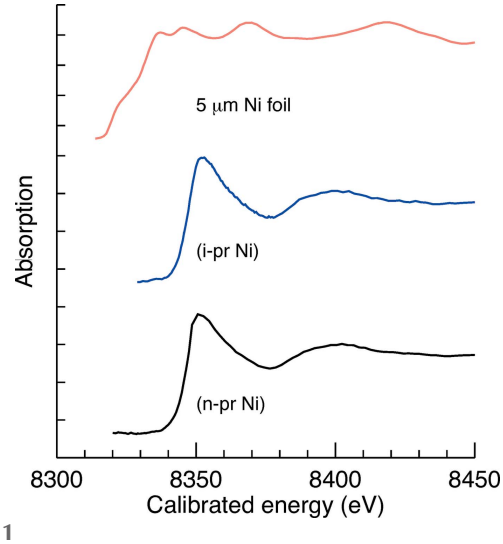

Figure 1
Absorption spectra of metallic Ni, bis(*N*-i-propyl-salicyldiminato) nickel(II) [(i-pr Ni)] and bis(*N*-n-propyl-salicyldiminato) nickel(II) [(n-pr Ni)], corrected for systematic experimental errors and calibrated in energy.

2.1. XAFS spectra with experimental uncertainty

An *IFEFFIT*-like spline approach (Smale *et al.*, 2006) was used to remove background absorption to extract the oscillatory part of the XAFS spectra with the propagation of experimental uncertainty at measured energies. One of the useful aspects of this approach is the determination of XAFS spectra on an absolute scale at the measured energies without interpolation over a fine energy grid to present the quality of data. This is important for the refinement of XAFS parameters using theoretical XAFS standards (multiple-scattering paths) for a given structure. The χ *versus* k spectrum, above the cut-off (threshold) energy E_0, and the corresponding uncertainty of χ are determined using

$$\begin{aligned} \chi &= \left[\mu(E) - \mu_0(E)\right]/\mu_0(E), \\ \sigma_\chi &= \sigma_{\mu(E)}/\mu_0(E), \end{aligned} \tag{1}$$

where $\mu(E)$ is the absorption as a function of energy, $\mu_0(E)$ is the background and σ_χ is the uncertainty of χ.

Theoretical XAFS spectra with the refined structures are shown by the red dashed lines in Fig. 2. A distortion in the XAFS oscillations is observed at higher k ($k > 10$ Å^{-1}), where the noise ratio begins to dominate.

3. Room-temperature crystal structures of the complexes

The crystal structural determinations of (i-pr Ni) and (n-pr Ni) (Fox *et al.*, 1964; Britton & Pignolet, 1989) provide the starting point for the structural analysis. X-ray diffraction measurements have been performed on a needle-shaped crystal of (i-pr Ni) (Fox *et al.*, 1964), space group *Pbca* (orthorhombic, International Tables number 61). Unit-cell dimensions were found to be a = 13.219 (6), b = 19.697 (8) and c = 15.14 (2) Å. A total of 1282 unique reflections, of which a number of 979 had measurable intensities, provided an R-factor of 0.06 and found a distorted tetrahedral geometry, due to constraints imposed by the bite angle of the chelating groups. Key bonding parameters are given in Table 1.

Crystal X-ray diffraction (XRD) measurements on plate-shaped crystal samples of (n-pr Ni) using a graphite monochromator (Britton & Pignolet, 1989) provided a total of 1048 reflections providing an R-factor of 0.03. This study yielded a monoclinic space group ($P21/c$, International Tables number 14), a = 10.025, b = 10.067, c = 9.167 Å, with angles of the cell axes of α = 90, β = 100.26, γ = 90°. The interatomic distances were reported to be O—C1 = 1.318 (3) Å, C1α—C2 = 1.393 (4) Å. This corresponds to a geometry of the ligands about nickel as planar in the form of a rhombus ('square planar') (Britton & Pignolet, 1989).

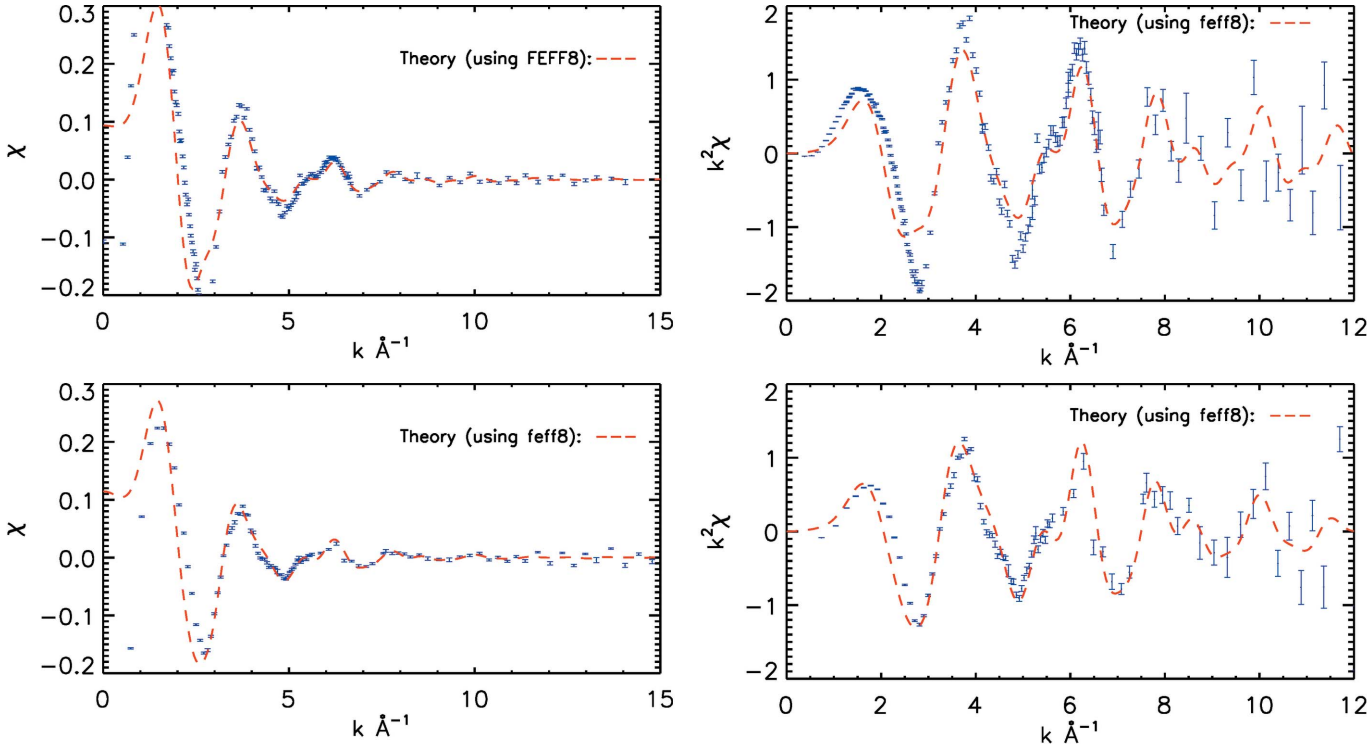

Figure 2
XAFS spectra of (i-pr Ni) (top row) and (n-pr Ni) (bottom row) determined on an absolute scale following the correction of the identified systematics addressed by Chantler *et al.* (2015). The red dashed lines are *FEFF8*-calculated theoretical XAFS using the models developed for the refinement of structural parameters of the complexes. While the functional uncertainty is difficult to view in the χ *versus* k plots, the strong information content at medium k and the onset of noise and lowering of information content is quite clear in the conventional $k^2\chi$ *versus* k plots, with the important difference that the derived uncertainties fairly represent the noise level. The XAFS oscillations are well defined up to k = 9–11 Å^{-1}. Higher measurement density or counting time at higher k can provide XAFS spectra with well defined accuracies for a larger range.

Table 1
Nearest-neighbour bond distances and angles based on the reported crystal structures with reported XRD uncertainties.

Refinement of standard XAFS parameters with the crystal structures led to erroneously high values of amplitude reduction factors S_0^2, possible expansion parameters α, unlikely values of E_0 and values of σ^2 discussed in the text. Despite this, fitted χ_r^2 values were of order 9, so that the crystal structure models in both cases were poor fits of the experimental XAS data. This could imply a false minimum, or incorrect (underestimated) uncertainties, but we demonstrate in this paper that this implies that interatomic structures of the crystals were changed or relaxed in solution. This analysis shows that there are differences in the relative Ni-scatterer contacts and/or thermal parameters between the crystal structure determinations and the observed solution data.

	(i-pr Ni)	(n-pr Ni)
Crystal bond distances and angles about Ni		
Ni—N2 (Å)	1.950 (9)	1.920 (2)
Ni—N1 (Å)	1.990 (5)	1.990 (5)
Ni—O1 (Å)	1.894 (5)	1.826 (2)
Ni—O2 (Å)	1.898 (4)	1.898 (4)
N1—Ni—O1 (°)	94.0 (2)	92.9 (1)
N2—Ni—O2 (°)	94.7 (3)	94.7 (3)
N1—Ni—N2 (°)	120.9	180
O1—Ni—O2 (°)	125.1	125.1
N1—Ni—O2 (°)	112.7	87.06
N2—Ni—O1 (°)	112.0	112.0
XAFS refined parameters using full crystal structures		
S_0^2	1.64 ± 0.38	2.04 ± 0.59
α	1.009 ± 0.014	1.057 ± 0.02
E_0	−8.89 ± −3.74	−8.17 ± 5.69
σ^2	0.008 ± 0.004	0.015 ± 0.006
χ_r^2	8.92	9.12
	Tetrahedral	Square planar

These two structures are not expected to be identical to the corresponding solution structures, quite apart from the disorder, the theoretical difference between mean-square lattice position and mean-square bond length and the structure of the environment. Several interesting questions arise: (i) Can we detect differences or variations of bond length or coordination due to the the different environment about the metal complex? (ii) Is XAFS sensitive in general to possibly small changes of bond length or angles compared with the crystalline moiety? (iii) How accurate were the structures of the crystalline forms, and can XAFS more incisively probe the bonding and local order? (iv) With the new transmission data from dilute frozen solutions across the available k-range, can we gain physical insight from the propagation of uncertainty to either validate or invalidate models which may be similar in form and which may preserve the prior understanding of the chemical ligands?

4. Refinement of XAFS using scaled X-ray structure models

With well defined experimental uncertainties, it is possible to test hypotheses, both standard and novel. We start by using the reported crystal structures to fit the experimental transmission XAS data for the (i-pr Ni) and (n-pr Ni) complexes. Table 1 gives the XAFS refinement parameters of the complexes using the full molecular structures of the complexes derived from the crystallographic determinations. If the intramolecular contacts are not significantly altered in a relative sense from the room-temperature crystal to the frozen solution, then the atomic coordinates can be used to model the XAFS with a single scale factor α, a single effective thermal broadening parameter σ^2, together with a definition of relative energy offset E_0 and the amplitude reduction factor S_0^2, giving a total of four fitting parameters.

In neither case does the refinement proceed to a satisfactory result, with fits of $\chi_r^2 \simeq 9$, with unphysical amplitude reduction factors. This is very clear because of the use of accurate estimates of uncertainty and error bars, which provide a reliable χ_r^2. High χ_r^2 can be due to the uncertainties being underestimated, but this is not the case as will be proven below. Instead, it confirms the widely held understanding that crystal-packing forces modify bond lengths and bond angles, that the environment of a molecule in an ordered *versus* disordered system affects its structure, and/or that the interatomic distances and angles appear to have changed or relaxed in solution.

Another potentially important question relates to the values of σ^2, the mean-square thermal displacements, sometimes known as the Debye–Waller factors and usually reported in crystallographic determinations as isotropic (scalar) or anisotropic (tensor) expectations of the displacements from the lattice sites due to a combination of static disorder (imperfections of the crystal) and dynamic disorder (thermal broadening). Here one must be careful as at least two conventions are used; nonetheless both crystal structures are consistent with equivalent values of B being of the order of 2.6 Å^2 for Ni, 3.9 Å^2 for oxygen, 2.7 Å^2 for nitrogen and 2.9–4.4 Å^2 for the range of carbon atoms, with perhaps 4.5 Å^2 for the hydrogen atoms, and with σ^2 values of the order of 0.04 Å^2. XAFS-fitted values are of the order of 0.01 Å^2, which is well explained: the crystals were measured at room temperature while the frozen solutions were at liquid-helium temperatures or of the order of 10 K. In some Debye models the value of σ^2 is approximately linear or quadratic with temperature, so the value seen at liquid-helium temperatures is almost completely determined by the static disorder. Hence the room-temperature crystal uncertainties, while consistent with the observed data at 10 K, cannot be used in any direct quantitative assessment of structure.

In this analysis, we use the approximation that all electron density scattering can be defined at the site of the nucleus of the atom rather than across the physical volume of the relevant bound electron wavefunction. However, within this isolated neutral atomistic interpretation, the crystallographic analysis demonstrates that the variation of thermal broadening (at room temperature) is within a factor of two for any of the atoms in the molecular unit, even including those for Ni and hydrogen. Hence, defining one effective thermal parameter as presented in Table 1 is a good first-order approximation, and we should expect correct values to vary broadening from specific sites within a factor of two of this assumption. Further, for static disorder (at 10 K) we might expect a similar value for all scatterers; or rather an increasing

disorder parameter with distance in a disordered environment such as a solution. Hence it is plausible that long scattering paths and multiple scattering paths (with more than two or three legs) should have an increased effective thermal parameter σ by a factor of $\sqrt{2}$, $\sqrt{3}$ or more, *i.e.* roughly within a factor of two.

The significance of crystal packing or relaxation may not seem a great revelation and is not that surprising, but here we are basing this observation upon, firstly, the resulting χ_r^2 arguing for a discrepancy between experimental data and model; secondly, the fitted parameter of S_0^2 appearing to be unphysical; and, thirdly, the fact that further investigation leads to a much improved result. Perhaps the most interesting aspect of this result is that it was obtained with transmission data from dilute disordered systems, and not from more conventional fluorescence data.

Having established the significant difference between the crystal structure and the solution data, one can question whether one should not just reject the crystal structure and begin in an *ab initio* approach to add one shell or one atom at a time. However, we have good confidence on the definition of the molecular composition and on the ligand shape, so it ought to be efficient and useful to investigate specific modifications of the reported crystal structures in order to find the unknown solution structures.

5. Can the distortions of the crystal structures be modelled by a relative rotation of the planes of the ligand? Is this significant?

If the ligand is considered to have a geometry defined by strong C—C, C—O and C—N bonds then a rotation of one of the ligands around the axis from the nickel atom through the bisector of the N and O atoms of the bidentate ligand may be a significant and possible distortion. Following the investigation of the crystal structures for XAFS modelling, we rotated the tetrahedral geometry towards square planar by rotating one of its two planes by angles of −10°, 10°, 80°, 90° and 100° and investigated whether this rotated tetrahedral structure might be a better fit to the so-called square planar (n-pr Ni) complex. This distortion links the tetrahedral and square planar forms. Table 2 shows the χ_r^2 produced from the XAFS modelling with the rotated geometries. Compared with the fit with its actual reported crystal ('square planar') geometry, the rotated tetrahedral geometries provided a significantly improved fit with lower χ_r^2, with a small statistical preference for the 90° rotation, pointing in fact to a square planar geometry but one quite different from the square planar crystal determination. The $\Delta\chi_r^2$ proved that this was a significant improvement over the use of the actual crystalline geometry for that complex (which was also planar). Possible reasons include the possibility that one structure might have been more carefully determined than the other, or that the tetrahedral structure had different bond lengths for the nearest neighbours whereas the planar structure had equal distances fixed by the crystal symmetry, and the influence of thermal parameters. This simple hypothesis test is of course independent of the search for the cause; it simply concludes that the derived structure is a better minimum and significantly improved match to the experimental data.

Table 2
Effect of ligand plane rotation on XAFS modelling of (n-pr Ni) and (i-pr Ni) commencing from the X-ray structures (Britton & Pignolet, 1989; Fox *et al.*, 1964) of the different isomers.

The rotation between the ligands was set to specific values and the refined values of $\chi_r^2 = 9.12$ and $\Delta\chi_r^2$ (relative to fits using the X-ray structure) reported improved fits with experiment for rotated geometries using the tetrahedral crystal at three different angles 90°, 80° and 100°. The $\Delta\chi_r^2$ values represent the difference (improvement) between the χ_r^2 with the actual crystal and the rotated tetrahedral model. The second part of the table reports the reverse rotation of the square planar towards the tetrahedral geometry, which shows no improvement at any angle of rotation.

Transmission XAFS of (n-pr Ni) (using the rotated tetrahedral crystal model)						
Rotation (°)	−10	0	10	80	90	100
χ_r^2	7.480	7.612	7.4057	7.392	7.364	7.386
$\Delta\chi_r^2$	1.64	1.51	1.714	1.728	1.756	1.734

Transmission XAFS of (i-pr Ni) (using the rotated square planar crystal model)						
Rotation (°)	−10	0	10	80	90	100
χ_r^2	10.02	10.69	10.20	9.83	9.66	9.78

The reversed hypothesis test is provided by taking the square planar crystal structure and rotating it towards a tetrahedral model, then fitting these to the (i-pr Ni) 'tetrahedral' complex. This indicates that one crystal structure fits the XAS data for both isomers much better than the other, and that there is a significant preference of the data for the expected tetrahedral or square planar geometries.

6. How much does the key bond length Ni—O shift in the minimization for the experimental data [(i-pr Ni), (n-pr Ni)]? Is it significant?

Refinement of the XAFS using the X-ray structures yields an effective scaling of all bond lengths in the *IFEFFIT*-like *fits* represented by α (Table 1), that is within an uncertainty of unity (1) for (i-pr Ni) but a significant positive scaling for (n-pr Ni) of 1.06 (2). While other fitted parameters were unphysical or implausible, the scaling for (n-pr Ni) improves the bond lengths of the crystal structure to agree more with those bond lengths of the (i-pr Ni) crystal structure. This is evidence that the success of the rotated tetrahedral crystal structure applied to (i-pr Ni) is because it is a more accurate and refined determination of relative positions and bond lengths of the core unit and less influenced by crystal packing. The scaling is dominated by the two distances Ni—O and Ni—N and particularly by the scaling of the Ni—O pair of distances due to the increased electron density around oxygen and due to the slightly shorter bond length.

7. How much does the key bond length Ni—N shift (in an absolute sense and also relative to Ni—O) in the minimization for the experimental data [(i-pr Ni), (n-pr Ni)]? Is it significant?

Table 3 shows the refinement statistics obtained from independently refined Ni—N and Ni—O distances following a grid search algorithm. Significant improvement was found with the increase of the key bond distances without changing other bonds or interatomic angles. Corresponding coordinate positions between the two planes (Fig. 3) of the tetrahedral geometry were not quite symmetrical. Key interatomic angles $N_{1,2}$—Ni—$O_{1,2}$ for the (i-pr Ni) crystal structure determined values were 94.0° and 94.6°.

Table 3
The χ_r^2 minimization by a progressive refinement of the key bond lengths of the reported tetrahedral (i-pr Ni) and square planar (rotated tetrahedral) (n-pr Ni) geometries.

A (non-uniform) increase or relaxation of the key bond distances improved the fits significantly over their crystalline geometries. Interatomic angles were not refined at this stage.

	Reported (Fox *et al.*, 1964) bond length (Å)	Tetrahedral XAFS (i-pr Ni)	Rotated tetrahedral (square planar) XAFS (n-pr Ni)
Ni—N1	1.950 (9)	1.993	1.911
Ni—N2	1.990 (5)	2.034	1.951
Ni—O2	1.894 (5)	2.011	1.868
Ni—O1	1.898 (4)	2.015	1.872
Energy offset (E_0)	–	−2.62 ± 1.02	−2.89 ± 1.26
Amplitude reduction factor S_0^2	–	1.27 ± 0.31	1.31 ± 0.34
Expansion coefficient α	–	1.001 ± 0.003	1.048 ± 0.015
Thermal parameter (σ^2)	–	0.005 ± 0.003	0.01 ± 0.004
χ_r^2	8.92 (Td); 9.12 (SQ)	5.47	6.17
$\Delta\chi_r^2$	–	3.45	2.92

Interestingly, the scaling on the (n-pr Ni) bond lengths is unity, $\alpha = 1.001$ (3); conversely, the value of $\alpha = 1.048$ (15) for (n-pr Ni) yields scaled bond lengths very similar to those for the (i-pr Ni) data. The bond lengths are stretched or relaxed in the frozen solution data sets compared with the crystallographic data. Using only the uncertainty from the (n-pr Ni) fit, of 1.5% or 0.030 Å, we can conclude that the (n-pr Ni) determination is consistent with that of the (i-pr Ni) determination and, therefore, for the (n-pr Ni) case at least, the results are consistent with a single Ni—N bond length and with a single Ni—O bond length. Conversely, the tetrahedral (i-pr Ni) system argues for *possibly* distinct Ni—N_1 and Ni—N_2 bond lengths.

It is quite plausible that the bonds in the solution might be stretched or relaxed by 2–5% compared with the crystal. It is interesting that these changes are not a uniform scaling but appear significantly different for the different bonds, and that the net result of this is a very significant reduction of χ_r^2 by 3–3.5 in both cases. The amplitude reduction factor is much more physical (though still high), the energy offset E_0 is now fairly consistent with theory to 1–2 eV, and the thermal parameters are broadly consistent. One difference between the XRD structures for (n-pr Ni) and (i-pr Ni) is the ratio of the Ni—N and Ni—O distances. It appears that this is better determined for (i-pr Ni) than for (n-pr Ni). This is a key parameter and provides very significant improvement in refinement statistics.

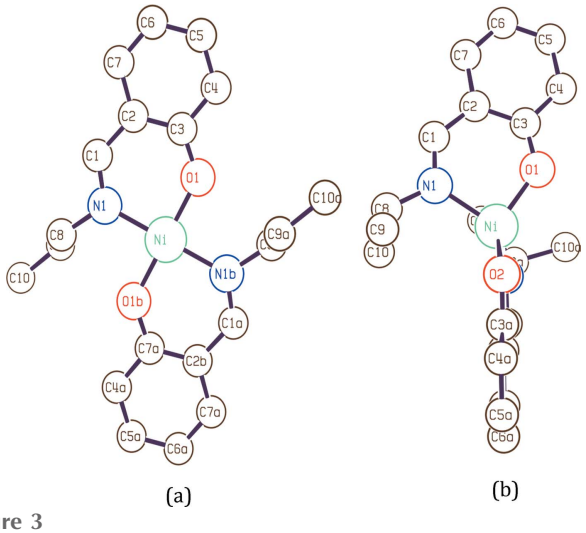

Figure 3
An *ORTEP* view of the reported crystal structures (Fox *et al.*, 1964; Britton & Pignolet, 1989) with tetrahedral and square planar geometries, excluding the hydrogen atoms from the plots, as summarized in Table 1.

8. Normalization of model structure for further XAFS modelling

There remain problems with the fitted structures reported in Table 3. The χ_r^2 values are significantly above unity indicating model error or uncertainty underestimation. A whole range of bond lengths and especially bond angles have not yet been optimized. Rather, a fixed ligand structure has been assumed as in protein crystallography but with no direct response to the change of environment from a crystal environment to a disordered solution. One might expect the two nitrogen atoms to be equivalent; and that the two oxygen atoms should be equivalent in solution; and that the two key bond angles (N_1—Ni—O_1 and N_2—Ni—O_2, for example) should be identical in solution, even if not in the crystal packing. Further, the modelling of thermal parameters in Table 3 is simplistic, and might be expected to be insufficient if the data quality is good over the relevant k range of XAFS fitting.

We therefore develop reduced XAFS models of the complexes using refined geometries. In searching for a solution to an XAFS or XANES data set, the researcher can use a true *ab initio* method (in principle) but normally will proceed with a prior or related structure before refinement. This can come from the crystal structure (of the actual molecule or related fragments) or other sources of structural information, *e.g.* calculations. Of these the crystallographic structure determination is usually considered the most robust and reli-

able, and we therefore have used it in this investigation. However, we now need to investigate chemical constraints or insight in order to approach the structure in its disordered environment.

A typical approach to XAFS model building is to compose the structure in layers of increasing distance from the absorbing atom reflecting the approximate $1/r^2$ dependence of the back-scattering intensity. Qualitatively this approach is well accepted. Therefore, at this stage, for XAFS modelling, we have developed a series of models informed by the fitted crystallographic structures and modified XAFS fits using symmetrized coordinate positions and fixed interatomic angles (Fig. 4).

Table 4
Refinement of the key bond lengths of model structure A (Fig. 4) to fit the experimental data with (i-pr Ni) and (n-pr Ni) complexes (R_{path} = 4.85 Å).

The constructed structure was used directly for a hypothesis test in fitting the experimental data, which produced a very poor fit. Refinement of the key interatomic distances improved the fit significantly. Refined bond lengths and XAFS parameters are listed. A single thermal parameter was used for all XAFS scattering paths.

	(i-pr Ni) initial values (Å)	(n-pr Ni) initial values (Å)	(i-pr Ni) refined values (Å)	(n-pr Ni) refined values (Å)
Bond length				
Ni—N_1, Ni—N_2	1.99	1.99	2.077 (4)	2.081 (4)
Ni—O_1, Ni—O_2	1.9	1.9	1.976 (4)	1.973 (4)
N—Ni—O	90°	90°	90°	90°
XAFS refined parameters				
S_0^2	1.45 ± 0.65	1.53 ± 0.62	0.999 ± 0.089	0.94 ± 0.12
α	1.028 ± 0.023	1.086 ± 0.023	1.0003 ± 0.004	1.012 ± 0.003
σ^2	0.009 ± 0.006	0.01 ± 0.01	0.0002 ± 0.0015	0.003 ± 0.002
E_0	−4.94 ± 6.44	7.62 ± 4.33	0.89 ± 0.87	3.7 ± 1.2
Returned χ_r^2	11.17	12.42	3.21	4.34
$\Delta\chi_r^2$	–	–	7.97	7.73

First, consider the model based upon a tetrahedral structure and the reported key bond lengths of Ni—O = 1.90 Å, Ni—N = 1.99 Å, N—C = 1.32 Å and O—C = 1.37 Å. Note that H atoms are omitted from this model (A) (Fig. 4*a*). The key interatomic bond angles forming the planes were fixed at 90°; this is 4° less than the reported angles (Fox *et al.*, 1964). A square planar model is similarly constructed with these corresponding bond lengths. We refined the key bond-distances to obtain the minimum χ_r^2 values and provide the results in Table 4. Initially the model is worse in most respects than the initial crystal structures, but the agreement is rapidly improved upon through refinement of the bond lengths.

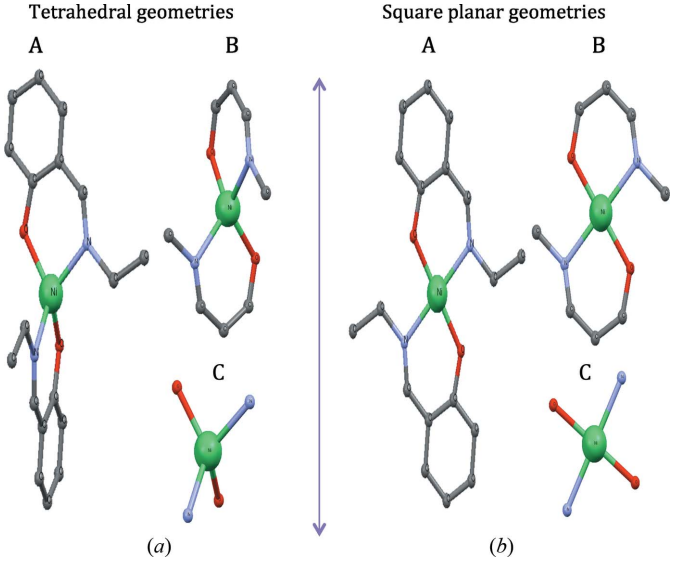

Figure 4
Illustrated models of the (i-pr Ni) and (n-pr Ni) complexes with geometries approximating tetrahedral and square planar, respectively (Fox *et al.*, 1963, 1964). Model A is a complete symmetrized molecule omitting the hydrogen atoms, Model B is the same omitting the second carbon ring, and Model C includes only the nearest neighbours.

The refined models are similar to one another in terms of fitted bond lengths, and similar to the earlier crystal-modified refinement, but now have common bond lengths for chemically identical species. Further, the amplitude reduction factor S_0^2 is now physical, and the energy offset is improved. The final χ_r^2 for each structure is now 3.2 and 4.3, significantly reduced from the previous minima of 5.5 and 6.2, respectively, from Table 3. Therefore these models are better representations of the experiment data and structure, with the exception that hydrogen atoms are omitted. Chemical ligand shape and structure is largely preserved between models, but some variations in structural parameters due to crystal packing for example no longer distort the structure, hopefully yielding a solution in better agreement with the actual unknown solution structure.

Having optimized bond distances for the given input interatomic angles of 90°, the key interatomic angles were then refined to give small changes in the bond distances and angles and significantly improved χ_r^2 (Table 5). The minima were found at N—Ni—O $\simeq$ 88.5 (4)° and 89.5 (5)° for (i-pr Ni) and (n-pr Ni), respectively, perhaps surprisingly lower than the corresponding crystallographic determinations (94.0° and 92.9°, respectively) and lower than the initial Model A default of 90°. Here the improvement with the optimization of bond lengths of Model A is large and significant, and the improvement with interatomic angle is quite different for the crystal structures but $\Delta\chi_r^2$ is only 0.5 or 0.9 compared with, for example, 93°. The interesting result is that the angular packing seems significantly different in the disordered solution, *i.e.* 94.0 (2)°, 94.6 (2)° and 92.9 (2)°, compared with the crystalline environment, 88.5 (4)° and 89.5 (5)°, respectively. In this case the formal uncertainties are about 0.5° but the valley of χ_r^2 is relatively shallow, and we have correlations between parameters. Hence, in Table 6 we refine the models assuming a bite angle of 93°. Results show useful improvement; but the minimum remains at bond angles of less than 90° rather than at the crystallographic values of 93–94°, with a significance

Table 5
Refinement of the key interatomic angles improved the fits using Model A, Fig. 4, with the coordination matching the expected complex.

The minima were found at approximately 88.5 (4)° or 89.2 (4)° and 89.5 (5)° for (i-pr Ni) and (n-pr Ni), respectively, perhaps suprisingly lower than the crystallographic determinations (94.0° and 92.9°, respectively) and lower than the initial Model A default of 90°. Improvement of χ_r^2 minimization is indicated by $\Delta\chi_r^2$. In both cases there is evidence but not proof of smaller bite angles for the ligands. The χ_r^2 of the best fit for each limiting geometry is shown in bold.

	θ = 89.2 (4)° (i-pr Ni)	θ = 91° (i-pr Ni)	θ = 92.0° (i-pr Ni)	θ = 93.0° (i-pr Ni)	θ = 89.5 (5)° (n-pr Ni)	θ = 91.0° (n-pr Ni)	θ = 92.0° (n-pr Ni)	θ = 93.0° (n-pr Ni)
Fitted parameters								
S_0^2	1.02 ± 0.03	0.97 ± 0.08	0.94 ± 0.12	0.98 ± 0.09	0.94 ± 0.11	0.915 ± 0.12	0.91 ± 0.12	0.91 ± 0.13
α	1.0022 ± 0.0062	1.005 ± 0.004	1.0014 ± 0.006	1.0012 ± 0.006	1.007 ± 0.0047	1.0143 ± 0.006	1.014 ± 0.007	1.0141 ± 0.007
σ^2	0.002 ± 0.002	0.002 ± 0.002	0.003 ± 0.002	0.003 ± 0.002	0.003 ± 0.002	0.003 ± 0.003	0.003 ± 0.003	0.003 ± 0.003
E_0	0.88 ± 0.78	1.21 ± 0.95	1.03 ± 0.96	1.3 ± 1.02	3.64 ± 1.36	3.97 ± 1.36	3.8 ± 1.3	4.09 ± 1.38
Returned χ_r^2	**3.18**	3.64	3.58	3.67	**4.25**	4.94	4.83	5.13

Table 6
Refinement of the key bond lengths (Ni—N and Ni—O) of a model by constraining their bite angles to 93°.

Interestingly, an increase in bite angle from 90° to 93° allowed further refinement of the bond lengths to slightly larger numbers.

	(i-pr Ni) initial values (Å)	(n-pr Ni) initial values (Å)	(i-pr Ni) refined values (Å)	(n-pr Ni) refined values (Å)
Bond length				
Ni—N_1, Ni—N_2	2.077	2.081	2.096 (5)	2.099 (4)
Ni—O_1, Ni—O_2	1.976	1.973	1.985 (4)	1.986 (4)
N—Ni—O	93°	93°	93°	93°
XAFS refined parameters				
S_0^2	1.45 ± 0.65	1.53 ± 0.62	0.96 ± 0.095	0.91 ± 0.11
α	1.028 ± 0.023	1.086 ± 0.023	0.995 ± 0.005	1.009 ± 0.004
σ^2	0.009 ± 0.006	0.01 ± 0.01	0.002 ± 0.002	0.003 ± 0.003
E_0	−4.94 ± 6.44	7.62 ± 4.33	1.17 ± 1.06	3.87 ± 1.37
Returned χ_r^2	3.67	5.13	3.48	4.88
$\Delta\chi_r^2$	–	–	0.19	0.25

corresponding to $\Delta\chi_r^2$ = 0.3 or 0.63, respectively. In other words, this is strongly suggestive of, but not conclusive to, the interatomic angle. Searches of the crystallographic Cambridge Structural Database (CSD) revealed 1000 relevant salicyldiiminato Ni bite angles, with a mean angle of 93.5° and a standard distribution of about 1.4°, which is inconsistent with our fitted minimum. The CSD does report crystal structures with bite angles of approximately 90°, whether by error or for chemically significant reasons; this 3 standard deviation discrepancy of the N—Ni—O bond angle may also be explained by the solution environment (CSD searches return crystal structures, not solutions).

For (i-pr Ni), the best fit with a returned χ_r^2 = 3.18 was obtained from an increase of Ni—N by 4.6% and Ni—O by 4.1% compared with their initial values. For the (n-pr Ni) complex, a 5% increase of Ni—N and 4.1% increase of the Ni—O bonds provided the best fit with a minimum χ_r^2 = 4.25.

9. XAFS models using model structures of the complexes: the influence of outer shells

It is often asked in XAFS analysis what the sensitivity of a data set or the technique itself is to next-nearest neighbours, sites farther away, multiple scattering and even the environment. While the XAFS equations clearly include these effects, can they be isolated and observed? In all cases the significance of the refinement of a given parameter is represented by $\Delta\chi_r^2$.

To investigate the effect of second shells (carbon rings), we used the nearest-neighbouring geometries Model C, Fig. 4, and the partial molecules Model B, Fig. 4, to fit experimental data (Tables 7 and 8).

Table 7 lists the refined XAFS parameters using the nearest-neighbouring structures. While the χ_r^2 values are quite poor, the relative χ_r^2 suggests that the bond angles and multiple paths still play a role in the data and fits. The initial model has a quite implausible value of E_0, and the complexity of the information content in the experimental data simply cannot be modelled by Model C. The refined structure has adjusted the bond lengths of the nearest neighbours to attempt to match deviations from the experimental structure. While this has reduced χ_r^2 somewhat, it yields E_0 which are implausible. This is a cautionary note for attempts at an aufbau principle of *ab initio* XAFS refinement; the minimization of the extended structure is more likely to yield a true minimum.

The second key idea from this study is that, indeed, XAFS data are quite sensitive to the second shell, and to multiple scattering contributions. While multiple scattering and extended units have been implemented in various theoretical packages for many years now, it is only when a robust χ_r^2 is available (from the propagation of reliable correlated or uncorrelated uncertainties) that one can test the sensitivity to these components in a given problem or in a given data set.

Compared with the nearest-neighbour geometry, the partial molecule geometry (Model B) is fitted in Table 8 and is much improved, both in terms of the initial defined model and also in the refinement with adjustment of (core) bond lengths. The (i-pr Ni) data yield a suspicious E_0, but otherwise the refinements seem reasonable. Further, the χ_r^2 values, although quite

Table 7
Refined parameters using the nearest-neighbour geometry Model C, Fig. 4, excluding all carbon scatterers.

The fit of experimental data with the model excluding both C rings and atoms provides very poor agreement with experimental data for both (i-pr Ni) and (n-pr Ni) complexes, even after the refinement of bond lengths. It is no better than the structures from the crystallographic determinations. The energy offset is not plausible. For the refinement of the XAFS models with the reduced structure (Model C), the refined coordinates with the full structure were used as the initial coordinates, then further refined to investigate the effect of carbon rings.

	(i-pr) initial values (Å)	(n-pr) initial values (Å)	(i-pr) refined values (Å)	(n-pr) refined values (Å)
Bond length				
Ni—N1/Ni—N2	2.077	2.085	2.072 (4)	2.081 (4)
Ni—O1/Ni—O2	1.976	1.976	1.984 (4)	1.978 (4)
N—Ni—O	90°	90°	90°	90°
XAFS refined parameters				
S_0^2	0.99 ± 0.18	1.1 ± 0.3	0.98 ± 0.11	1.11 ± 0.31
α	0.98 ± 0.01	0.997 ± 0.023	0.99 ± 0.03	0.98 ± 0.02
σ^2	0.006 ± 0.003	0.005 ± 0.005	0.005 ± 0.004	0.007 ± 0.005
E_0	−14.36 ± 3.43	−17.73 ± 6.48	−8.63 ± 2.32	−13.92 ± 6.48
Returned χ_r^2	7.19	10.42	6.82	8.73
$\Delta\chi_r^2$	–	–	0.4	1.7

Table 8
Refined parameters using the partial molecule Model B, Fig. 4.

Initial values were taken from the Model A output results, including the carbon ligand positions. The XAFS models were characterized with four key parameters including effective thermal parameter σ^2; expansion coefficient (α); amplitude reduction factor (S_0^2) and energy offset (E_0). The effect of the second C rings and the C atoms on the XAFS refined parameters is investigated using this test. Exclusion of the carbon rings provided a poor fit with relatively larger χ_r^2 values for both (i-pr Ni) and (n-pr Ni) complexes. The interatomic angles were fixed at 90°.

	(i-pr) initial values (Å)	(n-pr) initial values (Å)	(i-pr) refined values (Å)	(n-pr) refined values (Å)
Bond length				
Ni—N1/Ni—N2	2.077	2.085	2.070 (4)	2.081 (4)
Ni—O1/Ni—O2	1.976	1.976	1.981 (4)	1.975 (4)
N—Ni—O	90°	90°	90°	90°
XAFS refined parameters				
S_0^2	0.98 ± 0.1	0.92 ± 0.12	1.003 ± 0.110	0.95 ± 0.13
α	0.99 ± 0.007	1.004 ± 0.003	0.996 ± 0.006	1.008 ± 0.007
σ^2	0.008 ± 0.004	0.003 ± 0.003	0.004 ± 0.003	0.005 ± 0.003
E_0	−3.47 ± 1.36	0.38 ± 0.28	−2.62 ± 1.32	0.083 ± 1.42
Returned χ_r^2	4.57	4.87	4.41	4.30
$\Delta\chi_r^2$	–	–	0.2	0.6

promising, are significantly worse than the implementation of Model A and refinement for (i-pr Ni) and slightly worse for (n-pr Ni). In other words, this specific pair of XAFS data sets are sensitive not only to the second shell and multiple scattering paths but also to the outer molecular shell in the fitting. Similarly the fitted value of E_0 is also sensitive to the range of scattering paths. Fig. 5 illustrates the final optimized models for both data sets with different interatomic angles.

One problem with the aufbau principle is that any partial molecule will not be electrically neutral, and the overall potential surface from theory cannot be properly minimized to represent the molecular species. Even the absence of hydrogen atoms can influence this, but we postpone that discussion to another time.

10. Sensitivity of the data sets to thermal parameters

A key parameter obtained from a XAFS refinement is the (isotropic) thermal parameter or mean square displacement σ^2, sometimes identified with a Debye–Waller factor, which broadens the XAFS spectra increasingly with increasing k or temperature. Multiple effective thermal parameters can be associated with multiple scattering paths, which can also be categorized in terms of single and multiple scattering paths to fit experimental data. Thermal parameters derived from X-ray diffraction or related crystal structure determination must be used with caution for XAFS, as discussed earlier. Values must be measured at equivalent temperatures or across the same range. With the compounds under investigation, the XRD evaluations at room temperature provide no insight into realistic σ^2 at 10 K; they only provide upper limits. If the temperatures are matched, the mean square displacement of an atomic site from a lattice position (due to static or dynamic disorder) can be identical to the relevant σ^2 of the bond length for XAFS modelling under specific circumstances.

In circumstances where there is correlated dynamic motion, for example, the thermal parameters can vary significantly. Further, σ^2 of the central atom from which the photoelectron is emitted and σ^2 of the scattering electron density (or atomic scatterer at some level of approximation) would be added in quadrature for any uncorrelated motion of the two, for all binary paths. For triangular paths the addition is more complex. We can investigate key details of this in the current study.

Up to this point in the analysis a single thermal parameter (mean square path displacement σ^2) was used to fit all scattering paths. This neglects significant chemical differences between the potentials of electron density around each atomic scatterer. That is, it neglects the different vibrational amplitudes of electron density around Ni, O, N and C and provides some effective mean displacement for all of them. *IFEFFIT* is unsuited to model this chemical complexity, but other packages including *Artemis, XFIT* and *EXCURVE*, some of which use *IFEFFIT*, have been organized to provide correlated thermal parameters based largely on the atomic (chemical) scattering site, so that for example one can have

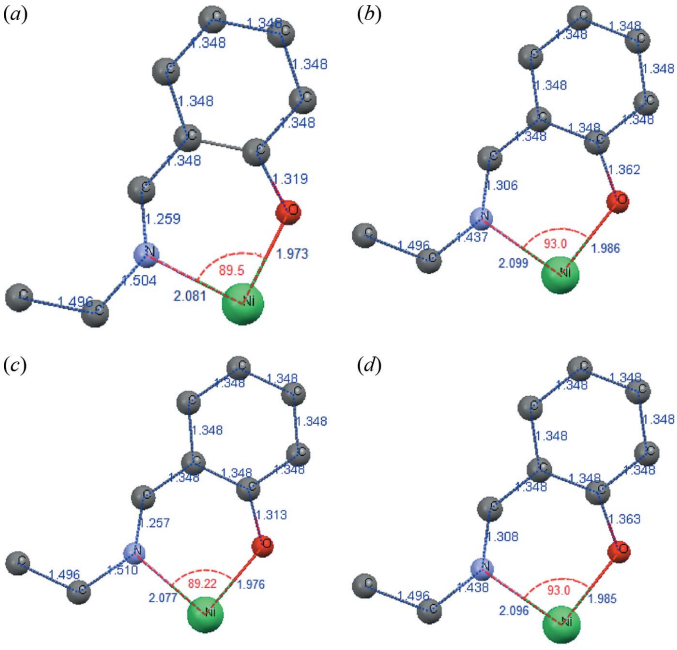

Figure 5
Key bond lengths and angles from XAFS analysis of (n-pr Ni) using the square planar model with: (*a*) the N—Ni—O angle refined in the analysis as 89.5°; (*b*) the N—Ni—O angle set at 93.0°; and XAFS analysis of (i-pr Ni) with (*c*) the N—Ni—O angle refined in the analysis as 89.2°; and (*d*) the N—Ni—O angle set at 93.0°.

effective isotropic thermal parameters for Ni—O, Ni—N and Ni—C independently.

With a single thermal parameter, the fitting of (i-pr Ni) returned χ_r^2 = 3.21 and (n-pr Ni) provided χ_r^2 = 4.34, or, with adjustment of bond angles, χ_r^2 = 3.18 and χ_r^2 = 4.25, respectively. Modelling with a single thermal parameter revealed that the theoretical XAFS did not properly converge with the experiment, particularly in the k = 5–6 Å^{-1} region for the (n-pr Ni) complex. It is therefore interesting to investigate whether the data set is in fact sensitive to the variations of (isotropic) thermal parameters from different chemical scatterers.

To do so, we refined the effective thermal factors corresponding to the Ni—N and Ni—O scattering paths, from the model relating to the full molecule (neglecting hydrogen atoms, Model A) and found σ^2 = 0.0010 ± 0.0005 for both N atoms and 0.00148 ± 0.00010 for both O atoms. For this purpose, as a guideline, we have used the program *XFIT* to model the mean square displacements particularly associated with the N and O atomic vibrations.

Now, restraining the refined thermal parameters of the *FEFF* scattering paths for Ni—N—Ni and Ni—O—Ni to these fitted values from *XFIT* modelling improved χ_r^2 to 2.94 and 3.27, respectively, or an improvement of $\Delta\chi_r^2$ = 0.24 and 1.0 (Table 9). While the former is a useful improvement it is not intrinsically significant, whereas the improvement for (n-pr Ni) is clearer and significant from the data set. It is useful to note that models fixing the interatomic angle to 93° are likewise improved by this procedure but still obtain a higher χ_r^2. One expects the thermal parameter σ^2 to be smaller for the two nearest, most correlated, paths; and that the effective thermal parameter for scattering density further away or from multiple paths to be larger and less correlated. Not only is this supported by the fits to the experimental data, but also all of the fitted magnitudes are reasonable, whether as an estimate from static or dynamic disorder.

One could imagine that, if the two most important paths are those for the scattering directly from oxygen and nitrogen nearest neighbours (true), then the next most important might be the scattering from the more distant carbon atoms, so that the effective thermal parameter here might be dominated by that of the Ni—C—Ni paths. It is also the case that the room-temperature crystal determinations returned a larger vibrational amplitude for the carbon atoms than for the Ni, N and O atoms. This element of the structure was modelled by the inclusion of a single σ^2 for all the paths involving the C atoms.

Table 9
Refined parameters by implementing multiple thermal parameters for the first- and second-shell scattering paths, following Table 5.

The tetrahedral model (Td) with a bond angle (N—Ni—O) of 89.2 (4)° and the square planar model (SQ) with a bond angle of 89.5° were used as the initial model. For comparison, similar models with an assumed bond angle of 93° are presented.

	(i-pr Ni) Td, N—Ni—O = 89.2°	(n-pr Ni) SQ, N—Ni—O = 89.5°	(i-pr Ni) Td, N—Ni—O = 93°	(n-pr Ni) SQ, N—Ni—O = 93°
Refined bond lengths				
Ni—N_1, Ni—N_2	2.077 (4)	2.081 (4)	2.096 (5)	2.099 (4)
Ni—O_1, Ni—O_2	1.976 (4)	1.973 (4)	1.985 (4)	1.986 (4)
Fitted parameters				
Effective thermal parameter (σ^2), Ni—N—Ni	0.0010 ± 0.0005	0.0010 ± 0.0005	0.0010 ± 0.0005	0.0010 ± 0.0005
Effective thermal parameter (σ^2), Ni—O—Ni	0.00148 ± 0.00010	0.00148 ± 0.00010	0.00148 ± 0.00010	0.00148 ± 0.00010
Amplitude reduction factor S_0^2	1.02 ± 0.02	0.91 ± 0.02	1.01 ± 0.03	0.89 ± 0.04
Expansion coefficient, α	1.0012 ± 0.0033	1.007 ± 0.003	0.998 ± 0.003	1.004 ± 0.006
σ^2, general paths	0.003 ± 0.002	0.006 ± 0.003	0.005 ± 0.002	0.007 ± 0.003
Energy offset (E_0)	0.62 ± 0.28	2.26 ± 1.14	0.87 ± 1.16	2.61 ± 1.46
Final χ_r^2	2.942	3.267	3.248	3.624
$\Delta\chi_r^2$	0.24	1.08		

Table 10
Investigation of the physical stereochemistry of complexes by cross-fitting optimized models.

XAFS refined structural parameters of (i-pr Ni) and (n-pr Ni) complexes as listed in parts (*a*) and (*b*), respectively. Experimental XAFS spectra for both (i-pr Ni) and (n-pr Ni) complexes were fitted using two different geometries: tetrahedral and 'square planar'. The fits confirm the correct and optimized stereochemistry. For comparison, refinement to analogous models with the O—Ni—N bite angle fixed at an average angle obtained from X-ray single-crystal crystallography (93°) are included to show that the conclusions are not dependent on the bite angle of the ligand.

	Theory model 1 (tetrahedral)	Theory model 2 (square planar)	Theory model 1A (tetrahedral)	Theory model 2A (square planar)
(*a*) (i-pr Ni) complex				
Fitted parameters				
Interatomic angle N—Ni—O	89.2°	89.5°	93°	93°
χ_r^2	2.94	5.42	3.25	4.97
Amplitude reduction factor S_0^2	1.02 ± 0.02	1.00 ± 0.21	1.01 ± 0.03	99 ± 0.09
Expansion coefficient α	1.0012 ± 0.0033	1.018 ± 0.007	0.998 ± 0.003	1.001 ± 0.005
Thermal parameter (σ^2)	0.003 ± 0.002	0.0023 ± 0.002	0.005 ± 0.002	0.002 ± 0.002
Energy offset (E_0)	0.62 ± 0.28	4.76 ± 1.64	0.87 ± 1.16	2.84 ± 1.08
(*b*) (n-pr Ni) complex				
Fitted parameters				
χ_r^2	4.72	3.27	4.74	3.62
Amplitude reduction factor S_0^2	0.93 ± 0.13	0.91 ± 0.02	0.84 ± 0.06	0.89 ± 0.04
Expansion coefficient α	1.008 ± 0.005	1.007 ± 0.003	0.999 ± 0.005	1.004 ± 0.006
Thermal parameter (σ^2)	0.002 ± 0.002	0.006 ± 0.003	0.006 ± 0.003	0.007 ± 0.003
Energy offset (E_0)	1.95 ± 1.26	2.26 ± 1.14	2.78 ± 1.22	2.61 ± 1.46

The energy offsets after inclusion of two effective thermal parameters seem quite reliable, namely that the energy calibration of the data set is indeed at the level of accuracy claimed, or about 0.5–1 eV. Our data sets claim accuracies of 0.1–0.2 eV, but the uncertainty of determining or fitting E_0 is greater than this value. One concern is the amplitude reduction factor S_0^2 for the (i-pr Ni) complex, which is slightly high and appears correlated with the imputed bond angles. This does not seem to be a problem for the 'square planar' (n-pr Ni) complex.

11. Sensitivity of the data sets to the symmetry of the environment: distorted tetrahedral or 'square planar'

Following §8–§10 (the refinement of the key bond lengths, angles, investigation of the effect of the outer shells and carbon rings, and the use of three effective thermal parameters), the best fitted models (with full molecular structures, Model A) were used to distinguish between the stereochemistry of the (i-pr Ni) and (n-pr Ni) complexes. For this purpose, both final models were used to fit the experimental XAFS of both complexes. In all fittings, the windowing was kept at k = 3.3–9 Å^{-1} (Table 10). This limited k range of fitting and data does distinguish between a distorted tetrahedral structure and a 'square planar' (rhombus) structure. In particular, the purported tetrahedral complex (i-pr Ni) is far better fitted with a distorted tetrahedral model ($\Delta\chi_r^2$ = 2.48); and the purported square planar complex (n-pr Ni) is far better fitted with a distorted square planar model ($\Delta\chi_r^2$ = 1.45). In other words, accurate XAS in absorption for m*M* solutions can readily discriminate between coordination and stereochemistry of nearest neighbours if uncertainties are propagated.

12. Parameterization in *FEFF* calculations

For consistent comparison, theoretical standards and fitting arguments for XAFS were determined with the same inputs, and parametrization throughout this analysis. However, different theoretical packages will certainly return different goodness-of-fits and different fitted parameters and uncertainties (if uncertainties can be propagated through the analysis). For example, the use of the *FEFF8* calculated scattering paths with the complete structures improved the fits significantly with lower χ_r^2 values compared with *FEFF6*. For calculating scattering paths (theoretical standards), an effective keyword in *FEFF8* is *RPATH*, the half-maximum path length of a scattering path. A given value of the keyword can be based on the cluster size of the molecule to produce or control the required scattering paths in modellng the experimental XAFS. Another important keyword is *NLEG*, which provides the maximum number of multiple scattering segments to be computed to determine the total number of paths between atomic electron density scatterers. Variation of these and other theoretical inputs changes the level of agreement with experiment, the returned parameters and uncertainties, and the goodness-of-fit.

This analysis found that the final model and XAFS minimization is sensitive to the parameterization of these two particular keywords (and to the version of *FEFF*). However, selection of *NLEG* across a broad and sensible range, *i.e.* 6–8, and *RPATH* in the range 4.75–4.90 Å, provided reasonable stability in XAFS models and refinement for both (n-pr Ni) and (i-pr Ni). These values for *RPATH* appear appropriate to include most of the molecular structure including the carbon rings, and to allow for multiple scattering from at least 3–4 paths as necessary for convergence. If these parameters are reflections of the convergent application of theory and experiment, then it is an indication that the XAFS data sets

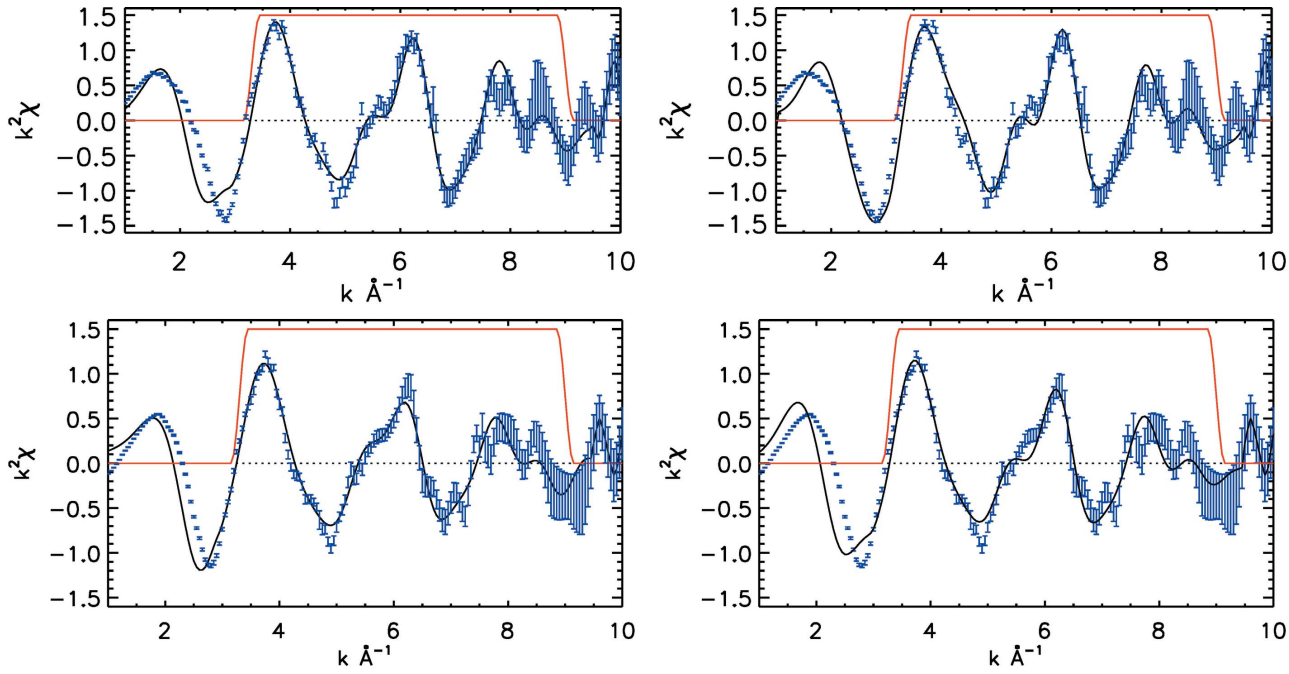

Figure 6
(Top left) Fitted $k^2\chi$ *versus* k plot of the (i-pr Ni) complex using the optimized tetrahedral geometry. This model provided the best fit with $\chi_r^2 = 2.94$. All figures use a window region k = 3.3–9 Å^{-1}. In the high-k region *IFEFFIT* automatically provides a uniform interpolated grid for theoretical modelling. (Top right) Fitted $k^2\chi$ *versus* k plot of the (i-pr Ni) complex using the optimized 'square planar' geometry yielding a poor fit with $\chi_r^2 = 5.42$. (Bottom left) Fitted $k^2\chi$ *versus* k plot of the (n-pr Ni) complex using the optimized 'square planar' geometry with the best fit with $\chi_r^2 = 3.27$. (Bottom right) Fitted $k^2\chi$ *versus* k plot of the (n-pr Ni) complex using the optimized tetrahedral geometry with a poor fit $\chi_r^2 = 4.72$. While the differences can be subtle to the eye, they are highly significant and well defined by the error analysis.

are really sensitive to the contributions from the carbon rings, as observed, and to multiple scattering.

13. Discussion of final fit and parametrization

Fig. 6 represents the final fits of the complexes following the refinement of bond distances, angles and implementation of multiple thermal parameters. The models do not include the hydrogen atoms, but otherwise represent a full molecule. Fig. 7 indicates the simulated differences as a function of k, showing small but significant differences across the full range of k.

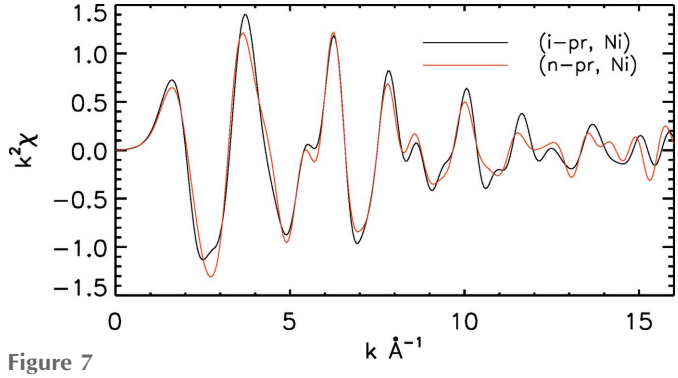

Figure 7
A signature of the theoretical *FEFF8* prediction of the difference between the isomers of the nickel(II) complexes in terms of XAFS signal. These subtle differences are seen in the experimental data sets. XAFS refined structures can be sensitive to and can reveal the stereochemical differences between isomers.

14. Data from pre-edge structural analysis

For centrosymmetric complexes the 1*s*–3*d* pre-edge transition is Laporte forbidden and weak, but for non-centrosymmetric tetrahedral complexes the transition is not forbidden and can have significant intensity. On this basis a significant difference in the relative intensities of the pre-edge transitions of (n-pr Ni) and (i-pr Ni) is expected. It is clear from the spectra (Fig. 8) that this expectation is unfulfilled. The explanation for this observation is unclear, but may be related to the strong overlap of metal and ligand orbitals which may result in molecular orbitals with significant metal 4*p* character at

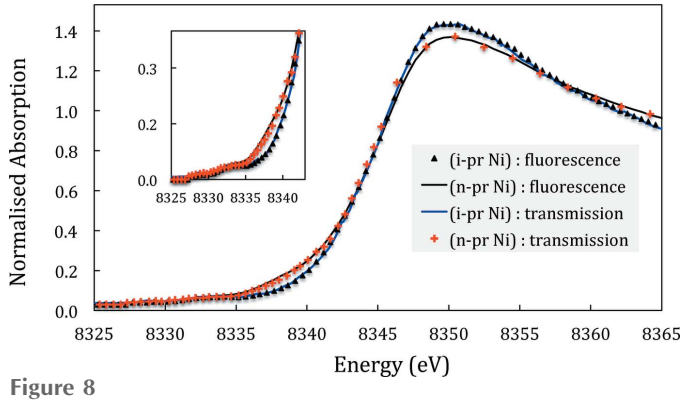

Figure 8
Pre-edge X-ray absorption spectra of (i-pr Ni) and (n-pr Ni) complexes as compared using data from both QuickXAFS and transmission hybrid XAS. The QuickXAFS data set is discussed and presented in Appendix *A* and is shown to demonstrate the reproducibility of the observation.

energies overlapping those of the Ni 3*d* orbitals. This would diminish significantly the difference in pre-edge intensities for the square planar and tetrahedral forms. These observations clearly demonstrate that structural conclusions based on the pre-edge intensities need to be treated with caution. It is important to note that careful analysis of the XAFS, while more demanding, leads to more reliable structural conclusions, even for equilibria between square planar and tetrahedral metal complexes.

The chemical shift $\Delta E = E_{K(\text{compound})} - E_{K(\text{metal})}$ is an important parameter which relates to the stereochemistry of a complex. It can be modelled to determine chemical information relating to the coordination of transition metal complexes (Furenlid *et al.*, 1995; Wakita *et al.*, 1993; Joshi & Shrivastava, 2006). Fig. 8 and Table 10 show a signature of the chemical shift of the complexes relative to the XAFS of their absorbing metal. The *K*-edge energies were found to be E_0 = 8331.01 eV for the ideal Ni element; E_0 = 8347.72 eV for the (i-pr Ni) complex; E_0 = 8348.52 eV for the (n-pr Ni) complex, yielding chemical edge-shifts of 16.71 eV and 17.51 eV, respectively. Accurate determination of E_K (compound data) requires accurate XAFS with calibrated energies or identical systematic corrections of experimental data, and simultaneous XAFS measurements with both the complex and the corresponding element under the same experimental conditions. The hybrid methodology provides the requirements, thereby yielding reliable chemical shift of the complex.

15. Results and discussion

While the general features of the structural chemistry of (n-pr Ni) and (i-pr Ni) in the solid state are retained in solution, careful analysis of the XAFS of frozen solutions of the compounds show that:

(i) The (i-pr Ni) complex has a distorted tetrahedral structure, while the (n-pr Ni) complex has a distorted 'square planar' structure.

(ii) The refined structural parameters reveal significant deviations from those obtained from X-ray crystal structure determination. These structural differences may be due to crystal packing or disorder of the molecules within the crystal.

(iii) The thermal σ^2 values can be different for different paths and this must be incorporated into accurate XAFS analysis.

(iv) The availability of accurate data with properly defined errors is necessary to make quantitative (and possibly qualitative) structural interpretation for XAFS results.

We find that one of the crystal structures matches relatively poorly with the nearest-neighbour distances and angles of the XAS data sets. The other is an excellent starting point for XAS analysis, and we find 10–16 standard error shifts of the Ni—O bond length from Table 1 to Tables 4, 5 and 8: from Ni—N 1.950 (9) Å, 1.990 (5) Å; Ni—O 1.894 (5) Å, 1.898 (4) Å to (i-pr Ni) Ni—N 2.077 (4) Å × α [1.0012 (33)] = Ni—O 1.976 (4) Å; (n-pr Ni) Ni—N 2.085 (4) Å × α [1.011 (6)] = Ni—O 1.976 (4) Å. One expects the solution to have longer bond lengths; and that the two Ni—N or Ni—O bonds should be identical within uncertainty, as observed in the XAFS solution data. Conversely, one could postulate that the 10 K temperature should shorten the bonds in the frozen solution compared with those of room-temperature crystallography, but this is not observed.

The N_1—Ni—O_1, N_2—Ni—O_2 bond angles appeared to be 94.0° from the distorted tetrahedral crystal structure, but have been determined for the solution to be quite close to 90°. The values found from the 10 K XAFS determination are much smaller than those from the crystal structures at room temperature, as expected. σ^2 at room temperature for crystals *ca* 0.04 Å^2 to σ^2 at 10 K of 0.0010 (5) for Ni—N—Ni path; 0.00148 (10) for Ni—O—Ni path; 0.003 (2) for general paths (i-pr Ni) or 0.006 (3) (n-pr Ni). Perhaps the most significant achievement is that the unphysical initial fit values for the crystal structures, S_0^2 = 1.64 (38), 2.04 (59); E_0 = −8.89 (3.74) eV, −8.17 (5.69) eV; χ_r^2 = 8.92, 9.12, refine with optimization to (i-pr Ni) E_0 = 0.62 (28) eV, χ_r^2 = 2.94; (n-pr Ni) E_0 = 2.23 (1.12) eV, χ_r^2 = 3.18. Other intriguing questions which are not addressed by these data sets include the detailed characterization of the effect of the crystalline environment compared with that of the (frozen) solution. Further significant improvements in the data quality can be obtained in the future. This analysis suggests that the availability of such data would make possible the investigation of even more subtle structural investigations, most importantly the influence of the environment about the complex on the coordination environment of the metal.

APPENDIX *A*
QuickXAFS data

In addition to the actual transmission XAS used in this analysis following the new *hybrid technique* (Chantler *et al.*, 2015), we have performed 'quick' scans to collect transmission data in a fine grid using the same experimental geometry used for hybrid transmission XAS. This so-called 'QuickXAFS' was determined following the hybrid analytical methodologies and correction (Chantler *et al.*, 2015). However, the collection of QuickXAFS data does not allow for the characterization of experimental systematics as does the actual hybrid transmission measurements. Because the QuickXAFS data were collected using the same experimental geometry for the transmission measurements as those using hybrid methodology, the experimental systematics characterized for the hybrid data were able to be used directly for the correction systematics on the QuickXAFS data.

In the 8–9.3 keV energy region, measurements were made at 10 eV energy steps in the pre-edge region, and 0.2 eV around the edge increasing up to 5 eV in the high-k region, up to k = 16 Å^{-1}. A total of 340 energy step measurements were made in the k = 0–10 Å^{-1} region. Measurements were made at 0.1–0.3 eV energy steps in the $0 < k < 3$ Å^{-1} region; 0.3–1.5 eV energy steps in the 3 Å^{-1} $< k <$ 5 Å^{-1} region, and 1.5–4 eV energy steps in the 5 Å^{-1} $< k <$ 10 Å^{-1} regions for both complexes. A great advantage of the QuickXAFS approach is that it is more optimized (in this experiment) for a high point

spacing density in the critical 5 Å^{-1} < k < 10 Å^{-1} region, and that the time required might be half of that of the hybrid technique. A key limitation is that most of the systematic corrections must be derived from the hybrid analysis and applied to the QuickXAFS data, which increases the uncertainty; and the point accuracy in general is better from both statistics and systematics for the hybrid technique. What this means in practice is that both approaches are complementary and provide effectively independent verification of model fitting and model-based hypothesis testing to within their error bars.

Data sets were collected for both 15 mM (n-pr Ni) and (i-pr Ni) complexes using three independent scans. The uncertainty contribution from dark currents was determined using the interpolated dark currents from the hybrid measurements under the same experimental conditions. To correct for a linear energy offset (Figs. 9 and 10), due to hysteresis already calibrated in the hybrid data sets, we have scaled the 'quick' transmission XAS to the hybrid transmission XAS, pinned at the pre-edge region.

Following the same methodologies detailed by Chantler *et al.* (2015), we have modelled the solvent background as shown in Fig. 11 for the XAS of the (i-pr Ni) complex. To determine the thickness fraction $t_{\rm frac} = t_{\rm sample}/t_{\rm pure}$, we have used the intensity measurements with the pure solvent used for hybrid XAS of the 15 mM solution with the same experimental geometry. The fitted path lengths from the scaled solvent background of the 15 mM solution and the pure solvent were then used to derive the required thickness fraction and corresponding fitted uncertainties (Fig. 11). The detailed

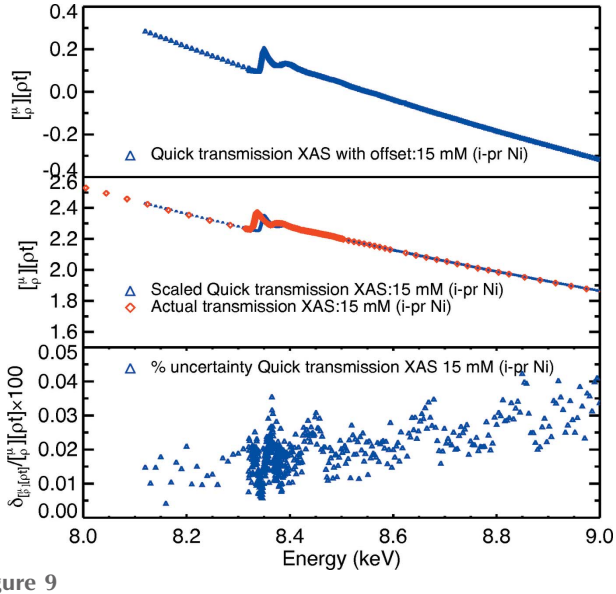

Figure 9
X-ray absorption spectra using the 15 mM solution with (i-pr Ni) from 'quick' scans. The uncertainty was determined from the variance of three independent scans, and including the variance of dark-current measurements made for the hybrid transmission XAS under the same experimental conditions. The quick transmission XAS for (i-pr Ni) was affected by detector gain change producing a linear offset, which was scaled with the hybrid transmission XAS determined with the same solution indicated by the red diamond markers.

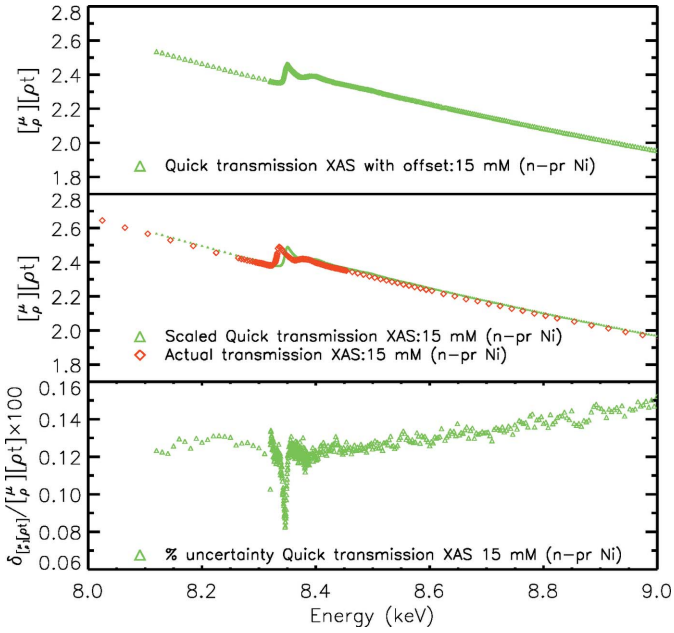

Figure 10
X-ray absorption spectra using the 15 mM solution with the (n-pr Ni) complex from quick scans. Note the higher level of noise in this data set, correctly treated to give a lower precision result.

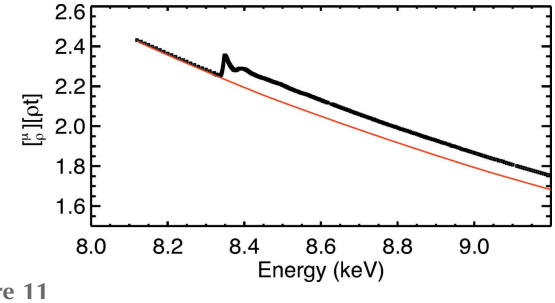

Figure 11
Modelled solvent background of the (i-pr Ni) complex.

methodology is given by Chantler *et al.* (2015). The fitted solvent background was then subtracted to determine the XAS of the solutes for both (i-pr Ni) and (n-pr Ni) complexes as shown in Figs. 12 and 13.

Key systematics including harmonic contamination and scattering contributions were corrected using the fitted values from the hybrid transmission measurements. A key systematic of solvent attenuation was characterized and corrected following the solvent modelling and correction procedure (Chantler *et al.*, 2015). The modelled active species of the QuickXAFS data is shown in Fig. 14. For calibrating energy, we have used calibrated energies from the hybrid transmission measurements.

We used the results of Figs. 1, 2, 5 and 6 from Chantler *et al.* (2015), unchanged, noting that this information was gained from the hybrid method, rather than the QuickXAFS method. Tables 1 to 5 are all in common for the two sets of data sets, being determined using the hybrid technique but being applied equally for the QuickXAFS technique. We used the results of Figs. 10, 11 and 12 interpolated from Chantler *et al.*

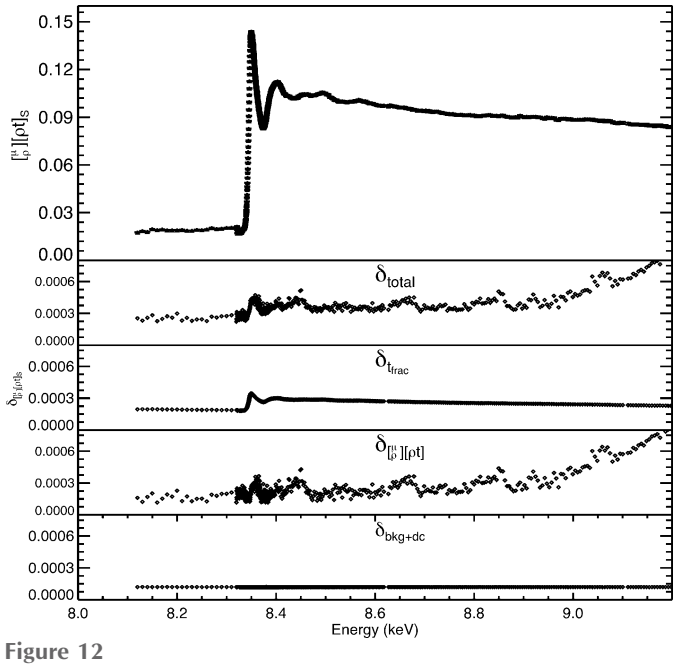

Figure 12
Solvent corrected XAS of the (i-pr Ni) complex, and corresponding uncertainties from different sources.

(2015). These uncertainties are dominated by the statistical precision and reproducibility of the QuickXAFS scans and not by the systematics, which have been determined quite accurately using the hybrid data sets. To determine the column densities, the fitted path lengths of the solutions were multiplied by the mass fractions of the solutions (Chantler *et al.*, 2015).

Table 11 confirms that the independent data set using QuickXAFS scanning, despite the quite different nature and distribution of uncertainties, also concludes that the crystal

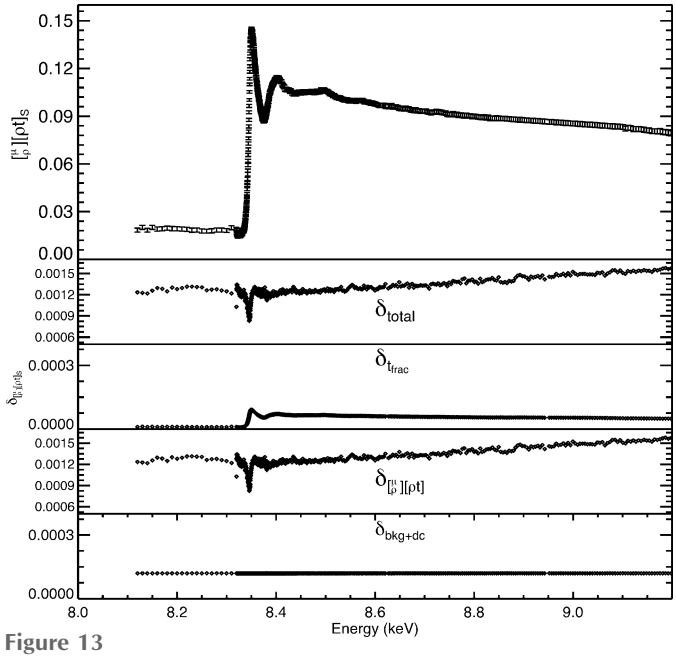

Figure 13
Solvent corrected XAS of the (n-pr Ni) complex, and corresponding uncertainties from different sources.

Table 11
QuickXAFS results, analogous to Table 1 for the hybrid data set.

Hypothesis test for XAFS modelling using the QuickXAFS transmission data set. Refinement of standard XAFS parameters with the crystal structures led to erroneously high values of amplitude reduction factors S_0^2, possibly plausible expansion parameters α, unlikely values of E_0 and values of σ^2 to be discussed in the text. Despite this, the final χ_r^2 values were of the order of 9, so that the crystal structure models in both cases were poor fits of the experimental XAS data. This is consistent with the analysis of the hybrid transmission XAFS.

	(i-pr)	(n-pr)
Bond distances and angles about Ni		
Ni—N2 (Å)	1.950 (9)	1.920 (2)
Ni—N1 (Å)	1.990 (5)	1.990 (5)
Ni—O1 (Å)	1.894 (5)	1.826 (2)
Ni—O2 (Å)	1.898 (4)	1.898 (4)
N1—Ni—O1 (°)	94.0 (2)	92.9 (1)
N2—Ni—O2 (°)	94.7 (3)	94.7 (3)
N1—Ni—N2 (°)	120.9	180
O1—Ni—O2 (°)	125.1	125.1
N1—Ni—O2 (°)	112.7	87.06
N2—Ni—O1 (°)	112.0	112.0
XAFS refined parameters using full crystal structures		
S_0^2	2.01 ± 0.86	2.71 ± 1.11
α	1.013 ± 0.012	1.045 ± 0.02
E_0	1.24 ± 3.74	−6.37 ± 4.93
σ^2	0.014 ± 0.004	0.0214 ± 0.007
χ_r^2	8.56	8.87

Table 12
QuickXAFS, analogous to Table 2, see main text.

Consistently, the use of the rotated tetrahedral crystalline geometry with the QuickXAFS transmission data improved the fit of experimental data for the (n-pr Ni) complex.

QuickXAFS			
Rotation (°)	80	90	100
χ_r^2	7.108	7.066	7.087
$\Delta\chi_r^2$	1.72	1.76	1.74

models from XRD are poor representations of the XAFS solution data, and therefore yield high χ_r^2 values. Also, similarly, and with a similar χ_r^2 reduction, the rotated tetrahedral structure serves as a better model for the distorted square planar complex (n-pr Ni) (Table 12). Again, Table 13 shows

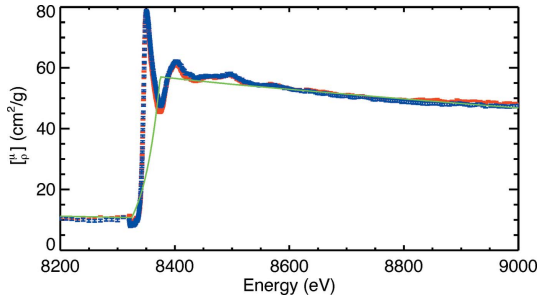

Figure 14
Comparison between $[\mu/\rho]$ of the two complexes. Blue points with error bars represent the (n-pr Ni) and the red points with error bars represent the (i-pr Ni) complexes. The corrected XAS (Figs. 12 and 13) were divided by the respective column densities $\{[\rho t]_{Td} = 0.0018421\ (18)$ and $[\rho t]_{SQ} = 0.0018721\ (23)\}$.

Table 13
QuickXAFS, analogous to Table 3, see main text.

Refinement of the key bonds using the QuickXAFS transmission data, which provides consistent parameters to the investigation of the hybrid transmission data sets. A (non-uniform) increase or relaxation of the key bond distances improved the fits significantly over their crystalline geometries.

	Reported (Fox *et al.*, 1964) bond length	Tetrahedral Q-XAFS (i-pr Ni)	Rotated tetrahedral (square planar) Q-XAFS (n-pr Ni)
Ni—N1	1.950 (9)	1.998	1.876
Ni—N2	1.990 (5)	2.040	1.917
Ni—O2	1.894 (5)	2.023	1.845
Ni—O1	1.898 (4)	2.027	1.849
Energy offset (E_0)	–	3.95 ± 3.21	−4.36 ± 3.52
Amplitude reduction factor S_0^2	–	1.31 ± 0.31	1.34 ± 0.37
Expansion coefficient α	–	1.007 ± 0.004	1.016 ± 0.014
Thermal parameter (σ^2)	–	0.007 ± 0.005	0.016 ± 0.005
χ_r^2	8.56 (Td); 8.87 (SQ)	5.17	5.63
$\Delta\chi_r^2$	–	3.39	3.24

Table 14
QuickXAFS: analogous to Table 7, see main text, Model C.

Refined parameters using Model C, Fig. 4, excluding all carbon scatterers. The fit of experimental data with the model excluding both C rings and atoms provides very poor agreement with experimental data for both (i-pr Ni) and (n-pr Ni) complexes, even after the refinement of bond lengths.

	(i-pr) initial values (Å)	(n-pr) initial values (Å)	(i-pr) refined values (Å)	(n-pr) refined values (Å)
Bond length				
Ni—N1/Ni—N2	2.077	2.085	2.081 (3)	2.102 (4)
Ni—O1/Ni—O2	1.976	1.976	1.979 (4)	1.993 (3)
XAFS refined parameters				
S_0^2	1.04 ± 0.31	1.3 ± 0.6	0.99 ± 0.23	1.2 ± 0.5
α	0.996 ± 0.02	1.02 ± 0.02	0.99 ± 0.02	1.01 ± 0.03
σ^2	0.006 ± 0.004	0.016 ± 0.011	0.006 ± 0.003	0.013 ± 0.014
E_0	−6.42 ± 4.42	−1.002 ± 4.271	−4.52 ± 4.42	−0.98 ± 3.21
Returned χ_r^2	7.18	9.74	6.94	8.48
$\Delta\chi_r^2$	–	–	0.2	1.3

significant improvement upon refining core bond-lengths, and the resulting parameters are generally within uncertainty of those using the hybrid data sets, with similar limitations at that stage of E_0, S_0^2 and σ^2. An argument would be that the fitting is robust, that these minima are global, and that the physical meaning and deficiencies are independent of the data set, as long as high-accuracy data sets with propagated uncertainties are used.

Fig. 15 and Tables 14 and 15 with the best fits plotted proves that these data sets are also sensitive to the structure of the C atoms and ligands in the second and third shells. Table 16 proves that the minimization of Model A, applied to the QuickXAFS data sets, was effective and that the optimization of bond lengths and bond angles of Model A also yields a dramatic improvement and consistent minimum for the QuickXAFS data sets in both cases, and that the data are sensitive to the use of three thermal parameters, as before. Once again, the solution for (i-pr Ni) is indeed distorted tetrahedral; and the solution found for (n-pr Ni) is indeed 'square planar' (a rhombus) and that the XAFS, although similar in shape, clearly demonstrate the local geometry. For the QuickXAFS data sets, the energy offsets are relatively poorly defined, as the mechanical hysteresis of the QuickXAFS scans was uncalibrated, as opposed to the hybrid approach. Further, the χ_r^2 values are closer to unity than for the hybrid data. This indicates that the data collected in each approach are reliable and consistent when calibrated for uncertainties, but that, despite the higher point density of measurement in energy and k-space, the hybrid data sets remain more sensitive to model inadequacies.

This analysis found that these QuickXAFS transmission data sets are consistent and complementary to hybrid transmission XAFS for structural analysis. However, to gain the accuracy from the QuickXAFS data set one requires the evaluation of systematics and uncertainties as is done for the hybrid data sets.

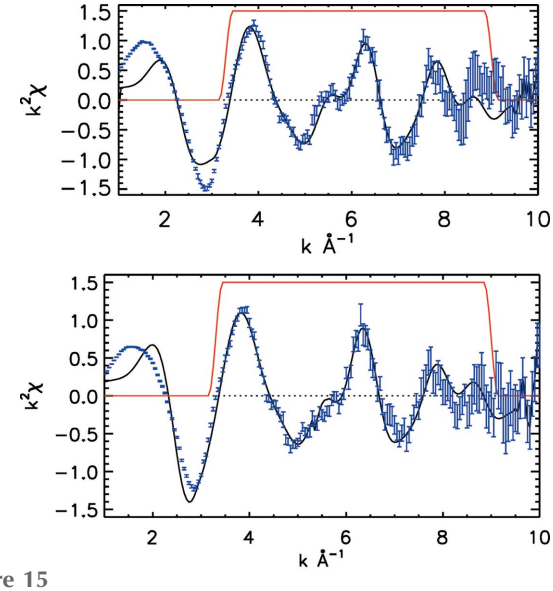

Figure 15
Final fitted XAFS models using QuickXAFS data of the (i-pr Ni) (top) and (n-pr Ni) (bottom) complexes.

Acknowledgements

The Australian Research Council (ARC) and the science faculty of the University of Melbourne are acknowledged for funding this work. The authors would like to thank the staff of the Australian National Beamline Facility (ANBF), Tsukuba, Japan, where the experiment was performed,

Table 15
QuickXAFS: analogous to Table 8, see main text, Model B, Fig. 4.

Exclusion of the carbon rings provided poor fits with relatively larger χ_r^2 values for both (i-pr Ni) and (n-pr Ni) complexes.

	(i-pr) initial values (Å)	(n-pr) initial values (Å)	(i-pr) refined values (Å)	(n-pr) refined values (Å)
Bond length				
Ni—N1/Ni—N2	2.077	2.085	2.070 (4)	2.081 (4)
Ni—O1/Ni—O2	1.976	1.976	1.981 (4)	1.975 (4)
XAFS refined parameters				
S_0^2	0.92 ± 0.13	0.94 ± 0.14	0.91 ± 0.15	0.97 ± 0.21
α	1.002 ± 0.005	1.001 ± 0.001	0.992 ± 0.013	0.981 ± 0.011
σ^2	0.006 ± 0.005	0.009 ± 0.004	0.007 ± 0.005	0.009 ± 0.004
E_0	4.32 ± 1.62	0.42 ± 0.31	3.45 ± 1.32	0.52 ± 0.43
Returned χ_r^2	4.57	4.88	4.24	4.72
$\Delta\chi_r^2$	–	–	0.33	0.28

Table 16
Analogous to Table 10, see main text.

The fits clearly favoured the optimized structures reflecting the correct stereochemistry. The χ_r^2 of the best fit for each limiting geometry is shown in bold.

	Theory model-1 (i-pr Ni)	Theory model-2 (n-pr Ni)
(*a*) (i-pr Ni) complex		
Fitted parameters		
χ_r^2	**2.31**	4.98
Amplitude reduction factor S_0^2	0.92 ± 0.12	0.90 ± 0.17
Expansion coefficient α	1.0014 ± 0.0062	1.021 ± 0.008
Thermal parameter (σ^2)	0.006 ± 0.002	0.005 ± 0.004
Energy offset (E_0)	3.37 ± 1.17	5.82 ± 1.33
(*b*) (n-pr Ni) complex		
Fitted parameters		
χ_r^2	3.67	**2.87**
Amplitude reduction factor S_0^2	0.9 ± 0.1	0.98 ± 0.21
Expansion coefficient α	1.012 ± 0.006	1.0012 ± 0.006
Thermal parameter (σ^2)	0.004 ± 0.003	0.007 ± 0.003
Energy offset (E_0)	0.46 ± 0.08	2.94 ± 1.65

for their assistance. As the ANBF is now closed, we dedicate this work to the efforts of the Australian and Japanese scientists who have worked together to make the beamline and collaboration such a success.

References

Anderson, J. R. (1975). *Structure of Metallic Catalysts*, Vol. 379. London: Academic Press.

Barnea, Z., Chantler, C. T., Glover, J. L., Grigg, M. W., Islam, M. T., de Jonge, M. D., Rae, N. A. & Tran, C. Q. (2011). *J. Appl. Cryst.* **44**, 281–286.

Bart, J. C. (1986). *Adv. Catal.* **34**, 203–296.

Britton, D. & Pignolet, L. H. (1989). *Acta Cryst.* C**45**, 819–821.

Chantler, C. T. (2009). *Eur. Phys. J.* **169**, 147–153.

Chantler, C. T., Islam, M. T., Best, S. P., Tantau, L. J., Tran, C. Q., Cheah, M. H. & Payne, A. T. (2015). *J. Synchrotron Rad.* **22**, 1008–1021.

Chantler, C. T., Rae, N. A., Islam, M. T., Best, S. P., Yeo, J., Smale, L. F., Hester, J., Mohammadi, N. & Wang, F. (2012). *J. Synchrotron Rad.* **19**, 145–158.

Eisenberger, P. & Kincaid, B. (1978). *Science*, **200**, 1441–1447.

Fox, M. R., Lingafelter, E. C., Orioli, P. L. & Sacconi, L. (1963). *Nature (London)*, **197**, 1104.

Fox, M. R., Orioli, P. L., Lingafelter, E. C. & Sacconi, L. (1964). *Acta Cryst.* **17**, 1159–1166.

Furenlid, L. R., Renner, M. W. & Fujita, E. (1995). *Physica B*, **208–209**, 739–742.

Glover, J. & Chantler, C. (2009). *X-ray Spectrom.* **38**, 510–512.

Harper, J. K., Grant, D. M., Zhang, Y., Lee, P. L. & Von Dreele, R. (2006). *J. Am. Chem. Soc.* **128**, 1547–1552.

Islam, M. T., Tantau, L. J., Rae, N. A., Barnea, Z., Tran, C. Q. & Chantler, C. T. (2014). *J. Synchrotron Rad.* **21**, 413–423.

Joshi, S. & Shrivastava, B. (2006). *Radiat. Phys. Chem.* **75**, 1894–1900.

Langford, J. I. & Louër, D. (1996). *Rep. Prog. Phys.* **59**, 131–234.

Lytle, F., Sayers, D. & Stern, E. (1975). *Phys. Rev. B*, **11**, 4825–4835.

Mazzara, C., Jupille, J., Flank, A.-M. & Lagarde, P. (2000). *J. Phys. Chem. B*, **104**, 3438–3445.

Perutz, M., Samar Hasnain, S., Duke, P., Sessler, J. & Hahn, J. (1982). *Ultramicroscopy*, **9**, 31–36.

Smale, L. F., Chantler, C. T., de Jonge, M. D., Barnea, Z. & Tran, C. Q. (2006). *Radiat. Phys. Chem.* **75**, 1559–1563.

Steiner, T. & Saenger, W. (1992). *J. Am. Chem. Soc.* **114**, 10146–10154.

Takayanagi, K. (1985). *J. Vac. Sci. Technol. A*, **3**, 1502–1506.

Tantau, L. J., Chantler, C. T., Bourke, J. D., Islam, M. T., Payne, A. T., Rae, N. A. & Tran, C. Q. (2015). *J. Phys. Condens. Matter*, **27**, 266301.

Tran, C., de Jonge, M., Barnea, Z. & Chantler, C. (2004). *J. Phys. B*, **37**, 3163–3176.

Wakita, H., Yamaguchi, T., Yoshida, N. & Fujiwara, M. (1993). *Jpn. J. Appl. Phys.* **32**, 836.

Yamaguchi, T., Lindqvist, O., Claeson, T. & Boyce, J. (1982). *Chem. Phys. Lett.* **93**, 528–532.